AIAA JOURNAL
Vol. 32, No. 12, December 1994

Efficient Sensitivity Analysis for Rotary-Wing Aeromechanical Problems

Anne Marie Spence* and Roberto Celi†
University of Maryland, College Park, Maryland 20742

This paper describes a method for the calculation of the sensitivities of rotating blade root loads and hub loads to changes of blade design parameters using a chain rule differentiation approach. The algorithm exploits features of the formulation of the blade and fuselage equations of motion, and of the solution technique, to calculate the sensitivities at a fraction of the cost of an aeroelastic analysis. The mathematical model of the blade includes nonlinearities because of moderately large elastic deflections and the fuselage is described by nonlinear Euler equations, so that the resulting model is valid for both straight and turning flight. The results indicate that the semianalytical technique is very accurate and computationally efficient.

Nomenclature

$\boldsymbol{A}$	= aerodynamic contributions to the blade equations
B	= number of blades
$\boldsymbol{B}(\psi)$	= matrix of derivatives of blade and fuselage equations with respect to states
$\boldsymbol{d}, \boldsymbol{D}$	= derivative vectors and matrices
EI_2, EI_3	= flap and lag bending stiffnesses
$\boldsymbol{F}_I^m$	= rotating blade inertia forces
$\boldsymbol{I}$	= inertia contributions to the blade equations
l_i	= length of the ith blade finite element
$\boldsymbol{M}_I^m$	= rotating blade inertia moments
m	= blade mass per unit length
n_e	= number of finite elements used to model the blade
$\boldsymbol{P}_{Ii}$	= vector of nodal inertia loads for the ith element
$\boldsymbol{P}_I^m$	= vector of inertia loads for the mth blade
$\boldsymbol{P}_{Si}$	= vector of nodal structural loads for the ith element
p	= generic design parameter
p, q, r	= fuselage roll, pitch, and yaw rates
$\boldsymbol{p}_I, \boldsymbol{q}_I$	= distributed blade inertia forces and moments
$\boldsymbol{p}_S, \boldsymbol{q}_S$	= distributed blade structural forces and moments
p_{xI}, p_{yI}, p_{zI}	= components of $\boldsymbol{p}_I$ along rotating undeformed blade axes
p_{xS}, p_{yS}, p_{zS}	= components of $\boldsymbol{p}_S$ along rotating undeformed blade axes
$\boldsymbol{q}$	= vector of states
q_{xI}, q_{yI}, q_{zI}	= components of $\boldsymbol{q}_I$ along rotating undeformed blade axes
q_{xS}, q_{yS}, q_{zS}	= components of $\boldsymbol{q}_S$ along rotating undeformed blade axes
$\boldsymbol{S}$	= structural contributions to blade equations
u, v, w	= fuselage velocity components
x_0	= nondimensional spanwise coordinate
x_I	= chordwise offset of center of mass from the elastic axis

Greek Symbols

α, β	= angles of attack and sideslip
β_P	= precone angle
γ, η, ϕ	= Hermitian interpolation polynomials
θ, ϕ	= fuselage pitch and roll angles
$\theta_0, \theta_{1c}, \theta_{1s}$	= collective, lateral, and longitudinal cyclic pitch
θ_B	= built-in blade twist
θ_G	= total geometric pitch angle
λ	= steady inflow
μ	= advance ratio
Φ_i	= normal mode matrix for the ith element

Subscripts and Superscripts

F	= fuselage quantity
i	= element number index
j	= rotor mode number index
k	= quasilinearization iteration index
m	= blade number index
n	= harmonic number index
R	= rotor quantity
$(\,)_{,x}$	= derivative with respect to spanwise coordinate
$(*)$	= $\mathrm{d}(\ldots)/\mathrm{d}\psi$

Presented as Paper 93-1648 at the AIAA/ASME/ASCE/AHS/ASC 34th Structures, Structural Dynamics, and Materials Conference, La Jolla, CA, April 19–22, 1993; received Nov. 26, 1993; revision received March 14, 1994; accepted for publication March 14, 1994.

*ARO Graduate Fellow, Department of Aerospace Engineering. Member AIAA.

†Associate Professor, Department of Aerospace Engineering. Member AIAA.

Introduction and Problem Statement

In the last decade there has been an increasing interest in the application of formal numerical optimization techniques to various aspects of helicopter design. A considerable portion of the work in this area has been devoted to the optimization of main rotor blades for minimum vibratory loads, with a variety of behavior constraints such as frequency placement, aeroelastic stability, and performance. A comprehensive review of this work has been presented by Friedmann.[1]

The applications of numerical optimization to rotor design problems follow two basic approaches, namely 1) to leave unchanged the analysis used to calculate the behavior quantities of interest, or 2) to modify it so that not only the required behavior quantities, but also their sensitivities, or gradients, with respect to a set of design variables are calculated as an integral part of the analysis (design-oriented analysis).

The first approach is by far the most common, because it allows the use of existing analyses, which are often implemented in computer programs that have evolved over a long period of time and that are costly and impractical to modify. Following this approach, the basic analysis is coupled with the optimizer, either directly or indirectly, through an approximate problem generator. In the former case the optimization program calls the analysis program every time an evaluation of objective function and behavior constraints is required to select a search direction or perform a one-dimensional minimization along the search direction. When gradients are needed they are calculated by repeatedly calling the analysis program and using finite difference approximations. In the case of indirect coupling, the optimizer performs the various calculations on simple,

frequently updated approximations to the objective function and behavior constraints, which are typically linear polynomials obtained through truncated Taylor series expansions in terms of the design variables about the current design. A direct coupling of analysis and optimizer is prohibitively expensive for most rotorcraft design problems of practical complexity. The conversion to a sequence of approximate optimization problems is much more efficient, but can still be very costly because the derivative information required to build each approximate problem is generally obtained using finite difference approximations, and therefore requires a minimum of one additional analysis per design variable if only first-order sensitivities are used. A relatively large number of studies based on this approach have been published in the literature; Ref. 2 contains several representative articles.

The second approach consists of coupling with the optimizer, either directly or through an approximate problem generator, a design-oriented analysis which provides both behavior quantities and sensitivity information. This approach usually requires extensive modifications to the existing basic analyses and therefore it has been less popular in rotary-wing applications. Furthermore, portions of the derivations and of the coding may have to be repeated when a new design variable is identified. On the other hand, it results in far more efficient computer implementations because it is often possible to calculate the gradient of the behavior quantities with respect to each design variable for an additional cost that is only a small fraction of the cost of one analysis. This is accomplished by deriving analytic or semianalytic expressions for the sensitivities using chain rule differentiation, and appropriately reusing the results of intermediate steps already performed in the calculation of the basic behavior quantities. Only a very limited number of studies on this topic have appeared in the literature. The first design-oriented rotor aeroelastic analysis is due to Lim and Chopra,[3–5] who derived expressions for the sensitivity of hub loads and aeroelastic stability eigenvalues with respect to several blade design parameters. The blade equations of motion are formulated from Hamilton's principle in weak form, and are discretized using a finite element method both in space and time. The majority of the sensitivity calculations are carried out analytically. Lu and Murthy[6] present an alternative method for the calculation of analytic sensitivities of the stability eigenvalues with respect to a variety of blade and helicopter configuration parameters, and use it with a simplified rigid blade, coupled rotor-fuselage model. Another design-oriented analysis is presented by He and Peters,[7] in which sensitivities are provided for power required and vibratory hub loads. An interesting feature of this study is the derivation of analytic sensitivities of the rotor downwash, based on a finite state dynamic wake model.

In Refs. 8 and 9 an implicit or numerical formulation of the equations of motion has been proposed as a tool to build aeromechanical analyses that are easier to implement and modify than traditional ones. In this formulation the various algebraic expressions that make up the mathematical model are not expanded symbolically, but are assembled numerically as part of the solution process. The general objective of this paper is to propose this numerical formulation as a useful tool to build computationally efficient, design-oriented aeromechanical stability and response analyses for use in optimization applications. The specific objective of this paper is to describe a methodology for the calculation of sensitivities of the following behavior quantities: 1) loads at the blade root (defined in the blade rotating coordinate system), 2) loads at the hub (defined in the hub nonrotating coordinate system), and 3) modal load vectors which are the structural, inertia, and aerodynamic load vectors of the finite element rotor model, following a modal coordinate transformation and assembly. They represent a basic building block for the calculation of the sensitivity of the aeroelastic stability eigenvalues.

The resulting design-oriented analysis can describe the coupled rotor-fuselage-inflow trim and dynamics of an articulated or hingeless rotor configuration in straight flight or during steady turns.

Analysis Method

The coupled rotor/fuselage aeromechanic model used in this paper is described in Ref. 10 and only a brief description is provided here. The rotor blades are modeled as Bernoulli-Euler beams undergoing coupled flap-lag-torsional motion. Small strains and moderate elastic deflections are assumed, introducing nonlinearities in the equations of motion of the blade. A Drees-type inflow model is used. Although the model includes quasisteady stall and compressibility effects, the results presented in this paper are obtained using linear aerodynamics only. The nonlinear, partial differential equations of motion of the blade are discretized using a finite element formulation based on the Galerkin method of weighted residuals. The finite elements are assembled into a global model after a modal coordinate transformation is used to reduce the number of variables.

The implicit approach presented in Refs. 8 and 9 provides the formulation for the equations of motion of the blade. This approach eliminates the need for complex algebraic expansions of the various components of the nonlinear dynamic model of the blade by building all of the various portions of the finite element equations of motion numerically as part of the solution process.

The solution of the aeromechanic stability problem is comprised of two steps. In the first step, the trim state of the helicopter and the steady blade response are calculated. This provides the control settings and fuselage attitudes and rates for a given steady flight condition as well as the steady-state elastic deflections of the blade which represents the periodic equilibrium position of the blade. A brief summary of the trim procedure is presented here; details are given in Ref. 11. The determination of the trim state of the helicopter is accomplished by the simultaneous solution of two coupled sets of nonlinear algebraic equations.

The first set of equations describes the steady-state behavior of the rotor, and is obtained by transforming the nonlinear ordinary differential equations of motion of the blade into a set of nonlinear algebraic equations using a global Galerkin method. The second set of equations comprises the fuselage equations, including the six fuselage force and moment equations, the Euler rate equations, and certain kinematic relations that must be satisfied in a turn. A straight flight condition can be treated as a special type of turn with a turn rate of zero. For a given flight condition, the solution of the trim problem yields the steady-state values of main rotor and tail rotor pitch controls, fuselage angle of attack α and sideslip β, average inflow over the main and the tail rotor disks, fuselage pitch and roll attitude angles θ and ϕ, and roll, pitch, and yaw rates p, q, and r. The trim solution also provides the steady-state periodic motion of the blades in flap, lag, and torsion in the form of a truncated Fourier series. These quantities define the equilibrium position of the helicopter, and are provided to the aeromechanic stability portion of the analysis.

The second step in the solution of the aeromechanic stability problem is the evaluation of the coupled rotor-fuselage aeromechanic stability. In this step, the equations of motion of the coupled rotor-fuselage system are linearized about an equilibrium position and the stability of the resulting linear system with periodic coefficients is evaluated using Floquet theory. In this phase, quasilinearization is used to solve the system of nonlinear ordinary differential equations (ODE) that describe the motion of the blades and the fuselage. The quasilinearization procedure is a Newton-Raphson-type method which transforms the problem of solving a system of nonlinear ODE into that of solving a sequence of systems of linear ODE. The original nonlinear coupled rotor-fuselage system is linearized about the equilibrium position of the previous iteration to obtain the linear system at any given iteration. The sequence of linear solutions converges to the solution of the original nonlinear system. This solution yields the equilibrium position of the coupled rotor-fuselage system.

The aeroelastic equations of motion can be written as follows:

$$\boldsymbol{F}_{NL}(\boldsymbol{q}, \overset{*}{\boldsymbol{q}}; \psi) = \boldsymbol{A}(\boldsymbol{q}, \overset{*}{\boldsymbol{q}}; \psi) + \boldsymbol{I}(\boldsymbol{q}, \overset{*}{\boldsymbol{q}}; \psi) + \boldsymbol{S}(\boldsymbol{q}; \psi) = \boldsymbol{0} \quad (1)$$

where the vectors $\boldsymbol{A}$, $\boldsymbol{I}$, and $\boldsymbol{S}$ contain, respectively, the aerodynamic, inertia, and structural contributions to the equations of motion and the state vector $\boldsymbol{q}$ is partitioned as

$$\boldsymbol{q} = \begin{Bmatrix} \boldsymbol{q}_R \\ \boldsymbol{q}_F \end{Bmatrix} \quad (2)$$

where the vector $\boldsymbol{q}_R$ contains the rotor states and $\boldsymbol{q}_F$ contains the fuselage and dynamic inflow degrees of freedom. The rotor portion

of the state vector $\boldsymbol{q}_R$ is defined as

$$\boldsymbol{q}_R = \left[\boldsymbol{q}_R^1\ \boldsymbol{q}_R^2\ \cdots\ \boldsymbol{q}_R^j\ \cdots\ \boldsymbol{q}_R^{nm}\ \overset{*}{\boldsymbol{q}}_R^1\ \overset{*}{\boldsymbol{q}}_R^2\ \cdots\ \overset{*}{\boldsymbol{q}}_R^j\ \cdots\ \overset{*}{\boldsymbol{q}}_R^{nm}\right]^T \quad (3)$$

in which nm is the number of rotor modes retained and $\boldsymbol{q}_R^j$ is the vector containing the harmonic coefficients of the jth rotor mode such that

$$\boldsymbol{q}_R^j = \left[q_0^j\quad q_{1c}^j\quad q_{1s}^j\quad q_{2c}^j\quad q_{2s}^j\ \cdots\right] \quad (4)$$

The size of the vector $\boldsymbol{q}_R^j$ depends on the number of harmonics retained. For example, if two harmonics are retained the vector has ten elements. The total rotor portion of the state vector $\boldsymbol{q}_R$ has $2 * nm * (2 * nharm + 1)$ elements. The fuselage portion of the state vector $\boldsymbol{q}_F$ is

$$\boldsymbol{q}_F = \left[u\quad v\quad w\quad p\quad q\quad r\quad \theta\quad \phi\quad \lambda_0\quad \lambda_s\quad \lambda_c\right]^T \quad (5)$$

where u, v, and w are the fuselage forward, lateral, and vertical velocities; p, q, and r are the nondimensional roll, pitch, and yaw rates; θ and ϕ are the Euler pitch and roll attitudes; and λ_0, λ_s, and λ_c are the steady, sine, and cosine portions of the rotor inflow.

Eq. (1) can be expanded using a first-order Taylor series such that

$$\boldsymbol{F}_{NL}(\boldsymbol{q}, \overset{*}{\boldsymbol{q}}; \psi) \approx \boldsymbol{F}_{NL}(\boldsymbol{q}^k, \overset{*}{\boldsymbol{q}}^k; \psi) + \left[\frac{\partial \boldsymbol{F}_{NL}}{\partial \boldsymbol{q}}\right](\boldsymbol{q} - \boldsymbol{q}^k) + \left[\frac{\partial \boldsymbol{F}_{NL}}{\partial \overset{*}{\boldsymbol{q}}}\right](\overset{*}{\boldsymbol{q}} - \overset{*}{\boldsymbol{q}}^k) = 0 \quad (6)$$

where k refers to the kth iteration of the quasilinearization procedure. Substituting $\boldsymbol{q}^{k+1}$ for $\boldsymbol{q}$ and $\overset{*}{\boldsymbol{q}}^{k+1}$ for $\overset{*}{\boldsymbol{q}}$, Eq. (6) can be rewritten in first-order form as

$$\overset{*}{\boldsymbol{q}}^{k+1} = \boldsymbol{B}^k(\psi)\boldsymbol{q}^{k+1} + \boldsymbol{f}^k(\psi) \quad (7)$$

where

$$\boldsymbol{B}^k(\psi) = -\left(\left[\frac{\partial \boldsymbol{F}_{NL}}{\partial \overset{*}{\boldsymbol{q}}}\right]^k\right)^{-1}\left[\frac{\partial \boldsymbol{F}_{NL}}{\partial \boldsymbol{q}}\right]^k \quad (8)$$

$$\boldsymbol{f}^k(\psi) = \left(\left[\frac{\partial \boldsymbol{F}_{NL}}{\partial \overset{*}{\boldsymbol{q}}}\right]^k\right)^{-1}\left(-\boldsymbol{F}_{NL}^k + \left[\frac{\partial \boldsymbol{F}_{NL}}{\partial \boldsymbol{q}}\right]^k \boldsymbol{q}^k + \left[\frac{\partial \boldsymbol{F}_{NL}}{\partial \overset{*}{\boldsymbol{q}}}\right]^k \overset{*}{\boldsymbol{q}}^k\right) \quad (9)$$

and

$$\left[\frac{\partial \boldsymbol{F}_{NL}}{\partial \boldsymbol{q}}\right]^k = \left[\frac{\partial \boldsymbol{A}}{\partial \boldsymbol{q}}\right]^k + \left[\frac{\partial \boldsymbol{I}}{\partial \boldsymbol{q}}\right]^k + \left[\frac{\partial \boldsymbol{S}}{\partial \boldsymbol{q}}\right]^k \quad (10)$$

$$\left[\frac{\partial \boldsymbol{F}_{NL}}{\partial \overset{*}{\boldsymbol{q}}}\right]^k = \left[\frac{\partial \boldsymbol{A}}{\partial \overset{*}{\boldsymbol{q}}}\right]^k + \left[\frac{\partial \boldsymbol{I}}{\partial \overset{*}{\boldsymbol{q}}}\right]^k \quad (11)$$

The derivative matrices determined in Eqs. (10) and (11) are calculated using finite difference approximations.

Sensitivity Analysis

This section presents the methodology for the calculation of the sensitivity of the blade root load vector, hub load vector, and modal load vector to changes in a generic design parameter p. The derivation is shown in detail for the inertia load vector. The structural and aerodynamic load vector sensitivities are constructed in a similar manner. A complete description of all vectors and matrices is presented in Ref. 12.

Sensitivity of the Blade Root Loads

The total inertia load vector of the mth blade at the blade root (in the rotating frame) is given by

$$\boldsymbol{P}_I^m(\boldsymbol{q}, \overset{*}{\boldsymbol{q}}; \psi) = \int_0^1 \begin{Bmatrix} p_{xI} \\ p_{yI} \\ p_{zI} \\ q_{xI} + v_{,x}\, q_{yI} + w_{,x}\, q_{zI} \\ v_{,x}\, q_{xI} + q_{yI} - v_{,x}\, w_{,x}\, q_{zI} \\ w_{,x}\, q_{xI} + q_{zI} \end{Bmatrix} \mathrm{d}x_0 = \begin{Bmatrix} \boldsymbol{F}_I^m(\boldsymbol{q}, \overset{*}{\boldsymbol{q}}; \psi) \\ \boldsymbol{M}_I^m(\boldsymbol{q}, \overset{*}{\boldsymbol{q}}; \psi) \end{Bmatrix} \quad (12)$$

in which the integrand contains the components of the distributed inertia force and moment vectors $\boldsymbol{p}_I = p_{xI}\hat{\boldsymbol{e}}_x + p_{yI}\hat{\boldsymbol{e}}_y + p_{zI}\hat{\boldsymbol{e}}_z$ and $\boldsymbol{q}_I = q_{xI}\hat{\boldsymbol{e}}_x + q_{yI}\hat{\boldsymbol{e}}_y + q_{zI}\hat{\boldsymbol{e}}_z$, along the axes of a rotating, undeformed blade coordinate system, as shown in Fig. 1. The terms $v_{,x}$ and $w_{,x}$ are the lag and flap bending slopes. The inertia force and moment vectors for the mth blade are, respectively, $\boldsymbol{F}_I^m$ and $\boldsymbol{M}_I^m$.

The sensitivity of the blade root inertia vector $\boldsymbol{P}_I^m$ to changes in the generic design parameter p is determined using chain rule differentiation such that:

$$\frac{\mathrm{d}\boldsymbol{P}_I^m(\psi)}{\mathrm{d}p} = \underbrace{\frac{\partial \boldsymbol{P}_I^m(\psi)}{\partial p}}_{=\boldsymbol{d}_1} + \underbrace{\frac{\partial \boldsymbol{P}_I^m(\psi)}{\partial \overset{*}{\boldsymbol{q}}}}_{=\boldsymbol{D}_1}\underbrace{\frac{\partial \overset{*}{\boldsymbol{q}}}{\partial p}}_{=\boldsymbol{d}_2} + \underbrace{\frac{\partial \boldsymbol{P}_I^m(\psi)}{\partial \boldsymbol{q}}}_{=\boldsymbol{D}_2}\underbrace{\frac{\partial \boldsymbol{q}}{\partial p}}_{=\boldsymbol{d}_3} \quad (13)$$

The vector $\boldsymbol{d}_1$ is the sensitivity of the blade root inertia loads to changes in p for fixed normal modes and equilibrium position. This vector can be calculated in a simple and inexpensive way if an implicit formulation of the aeroelastic problem is used. Using Eq. (12) the vector $\boldsymbol{d}_1$ is given by

$$\boldsymbol{d}_1 = \frac{\partial \boldsymbol{P}_I^m}{\partial p} = \int_0^1 \begin{Bmatrix} \dfrac{\partial p_{xI}}{\partial p} \\ \dfrac{\partial p_{yI}}{\partial p} \\ \dfrac{\partial p_{zI}}{\partial p} \\ \dfrac{\partial q_{xI}}{\partial p} + v_{,x}\dfrac{\partial q_{yI}}{\partial p} + w_{,x}\dfrac{\partial q_{zI}}{\partial p} \\ v_{,x}\dfrac{\partial q_{xI}}{\partial p} + \dfrac{\partial q_{yI}}{\partial p} - v_{,x}\, w_{,x}\dfrac{\partial q_{zI}}{\partial p} \\ w_{,x}\dfrac{\partial q_{xI}}{\partial p} + \dfrac{\partial q_{zI}}{\partial p} \end{Bmatrix} \mathrm{d}x_0 = \begin{Bmatrix} \dfrac{\partial F_{xI}^m}{\partial p} \\ \dfrac{\partial F_{yI}^m}{\partial p} \\ \dfrac{\partial F_{zI}^m}{\partial p} \\ \dfrac{\partial M_{xI}^m}{\partial p} \\ \dfrac{\partial M_{yI}^m}{\partial p} \\ \dfrac{\partial M_{zI}^m}{\partial p} \end{Bmatrix} \quad (14)$$

Consider now, for example, the derivative $\partial p_{yI}/\partial p$. The inertia force component p_{yI} is given by[13]

$$p_{yI} = -m(a_{21} + a_{22}x_0 + a_{23}x_I\cos\theta_G + a_{24}x_I\sin\theta_G) \quad (15)$$

in which the as depend on parameters such as blade geometry, elastic deformations, and angular velocity, and are calculated at various blade stations and azimuth angles as required by the solution process. The total geometric pitch angle θ_G is defined as $\theta_G = \theta_0$

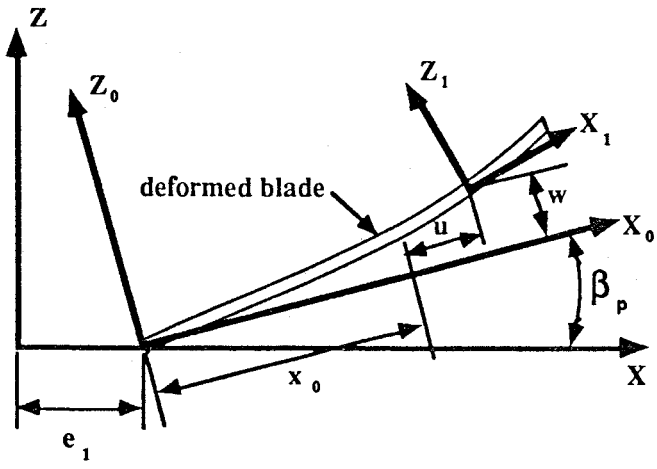

Fig. 1 Blade undeformed and deformed coordinate systems.

$+\theta_{1c}\cos\psi + \theta_{1s}\sin\psi + \theta_B$, with θ_B being the built-in twist. Thus, if the design parameter p is the mass m or the offset x_I then the sensitivities are given, respectively, by

$$\frac{\partial p_{yI}}{\partial m} = -(a_{21} + a_{22}x_0 + a_{23}x_I\cos\theta_G + a_{24}x_I\sin\theta_G) \quad (16)$$

$$\frac{\partial p_{yI}}{\partial x_I} = m(a_{23}\cos\theta_G + a_{24}\sin\theta_G) \quad (17)$$

Almost all of the computational effort in the calculation of the inertia loads goes into the calculation of the coefficients a_{ij}. Therefore, comparing Eqs. (16) and (17) with Eq. (15) it becomes clear that the sensitivities of the inertia loads contained in the vector $\boldsymbol{d}_1$ can be calculated with negligible additional cost for several design parameters of practical interest. The comparison also suggests that modifications of the mathematical model can be carried out with a modest implementation effort. For example, changes in the geometry or kinematic modeling of the blade would be reflected in the a_{ij} coefficients only. Therefore, once the procedure to calculate the a_{ij}s is appropriately changed to carry out the baseline aeroelastic analysis, no further changes would be required to calculate the sensitivities.

The coefficients a_{ij} implicitly depend on other configuration parameters that could also be used as design variables. These include blade hinge offset, precone, and sweep, and mast height and orientation. The sensitivities with respect to this set of design parameters require the derivatives of the a_{ij} coefficients. For example, the sensitivity of p_{yI} to the precone angle β_p would be given by

$$\frac{\partial \boldsymbol{p}_{yI}}{\partial \beta_P} = -m\left(\frac{\partial a_{21}}{\partial \beta_P} + \frac{\partial a_{22}}{\partial \beta_P}x_0 + \frac{\partial a_{23}}{\partial \beta_P}x_I\cos\theta_G + \frac{\partial a_{24}}{\partial \beta_P}x_I\sin\theta_G\right) \quad (18)$$

The derivatives of the a_{ij} coefficients can be obtained through chain rule differentiation of the expressions that are combined numerically to make up the nodal inertia vector.

The vectors $\boldsymbol{d}_2$ and $\boldsymbol{d}_3$ in Eq. (13) represent the sensitivity of the steady-state response of the blade to the design parameter p. These vectors can be calculated by perturbing the solution of the coupled rotor-fuselage trim problem, as follows. The state vector $\boldsymbol{q}$ corresponding to the steady-state periodic response of the blade in trimmed conditions is represented as

$$\boldsymbol{q}(\psi) = \left[\boldsymbol{q}_0 + \sum_{n=1}^{N}(\boldsymbol{q}_{nc}\cos n\psi + \boldsymbol{q}_{ns}\sin n\psi)\right] \quad (19)$$

The constant vectors $\boldsymbol{q}_0$, $\boldsymbol{q}_{nc}$, and $\boldsymbol{q}_{ns}$ are included in the unknowns of the trim problem and are provided as part of the solution. The size of each of these $2N + 1$ vectors is equal to the number of normal modes used in the modal coordinate transformation.

Then the sensitivity vector $\boldsymbol{d}_3$ can be written as

$$\boldsymbol{d}_3 = \frac{\mathrm{d}\boldsymbol{q}}{\mathrm{d}p} = \frac{\mathrm{d}\boldsymbol{q}_0}{\mathrm{d}p} + \sum_{n=1}^{N}\left(\frac{\mathrm{d}\boldsymbol{q}_{nc}}{\mathrm{d}p}\cos n\psi + \frac{\mathrm{d}\boldsymbol{q}_{ns}}{\mathrm{d}p}\sin n\psi\right) \quad (20)$$

A similar expression can be obtained for the vector $\boldsymbol{d}_2$. The derivatives in Eq. (20) can be obtained using finite difference approximations. For example,

$$\frac{\mathrm{d}\boldsymbol{q}_0}{\mathrm{d}p} \approx \frac{\boldsymbol{q}_0(p + \Delta p) - \boldsymbol{q}_0(p)}{\Delta p} \quad (21)$$

where Δp is a small increment of the design parameter p, and the notation $\boldsymbol{q}_0(p)$ emphasizes the dependence of the vector $\boldsymbol{q}_0$ on p.

The coupled rotor-fuselage trim problem consists of a set of nonlinear algebraic equations that, in the implementation of this model, are solved numerically using a quasi-Newton method. The solution process begins by generating an initial approximation to the Jacobian using a finite difference scheme. This approximation is then improved at each iteration using secant, rank-one updates, until convergence is reached. The calculation of the initial Jacobian is typically the most computationally expensive portion of the solution process, but it is not required for the solution of the perturbed problem, needed in Eq. (21). In fact, the secant approximation obtained at the end of the baseline trim solution can be used as a very good initial approximation in the solution of each of the perturbed trim problems. It is important to carry out the baseline trim solution to convergence. In fact, if the trim iterations are stopped prematurely, the perturbed solution may contain not only the changes caused by the perturbations of the design variable, but also unwanted changes due to the iterations left over from the unconverged baseline trim solution. Therefore the cost of determining the sensitivity of the trim solution with respect to each of the design parameters is a small fraction of the cost of solving the baseline trim problem which, in turn, is typically no more than 10–20% of the total cost of an aeroelastic stability and response analysis.

Finally, the matrices $\boldsymbol{D}_2$ and $\boldsymbol{D}_3$ in Eq. (13) represent the sensitivities of the blade root inertia loads with respect to the generalized coordinate vectors $\boldsymbol{q}$ and $\dot{\boldsymbol{q}}$. The calculation of these matrices would probably be the most time consuming portion of the sensitivity calculations, but when a quasilinearization solution procedure is used these matrices are already calculated as part of the solution process, and are available for the sensitivity calculation at no additional computational cost. The quasilinearization process uses the derivative matrices in Eqs. (10) and (11) which are determined from finite difference approximations. In order to determine $[\partial \boldsymbol{I}/\partial \boldsymbol{q}]^k$, the inertia loads at each spanwise integration point are first calculated. It is then simple to extract the derivative vector $\boldsymbol{D}_2$ before the spanwise inertia loads are transformed to modal inertia loads. No additional computations are required for the calculation of this portion of the sensitivities.

Sensitivity of the Hub Loads

Focusing, as in the previous sections, on the inertia loads, the resultant inertia hub force and moment vectors are defined in terms of their components along a system of hub-fixed, nonrotating axes, as shown in Fig. 2:

$$\boldsymbol{F}_I = F_{xI}\boldsymbol{i}_{\mathrm{NR}} + F_{yI}\boldsymbol{j}_{\mathrm{NR}} + F_{zI}\boldsymbol{k}_{\mathrm{NR}} \quad (22)$$

$$\boldsymbol{M}_I = M_{xI}\boldsymbol{i}_{\mathrm{NR}} + M_{yI}\boldsymbol{j}_{\mathrm{NR}} + M_{zI}\boldsymbol{k}_{\mathrm{NR}} \quad (23)$$

The inertia hub loads in the fixed frame can be written in terms of the blade root inertia loads as follows:

$$\begin{Bmatrix} F_{xI}(\psi) \\ F_{yI}(\psi) \\ F_{zI}(\psi) \end{Bmatrix} = \sum_{m=1}^{B}\begin{bmatrix} -\cos\psi_m & \sin\psi_m & 0 \\ \sin\psi_m & \cos\psi_m & 0 \\ 0 & 0 & -1 \end{bmatrix}\begin{Bmatrix} F_{xI}^m(\psi) \\ F_{yI}^m(\psi) \\ F_{zI}^m(\psi) \end{Bmatrix} \quad (24)$$

$$\begin{Bmatrix} M_{xI}(\psi) \\ M_{yI}(\psi) \\ M_{zI}(\psi) \end{Bmatrix} = \sum_{m=1}^{B}\begin{bmatrix} -\cos\psi_m & \sin\psi_m & 0 \\ \sin\psi_m & \cos\psi_m & 0 \\ 0 & 0 & -1 \end{bmatrix}\begin{Bmatrix} M_{xI}^m(\psi) \\ M_{yI}^m(\psi) \\ M_{zI}^m(\psi) \end{Bmatrix} \quad (25)$$

where m refers to the mth blade in the rotating frame, and the notation showing the dependence on the generalized coordinate vector $\boldsymbol{q}$ has been omitted.

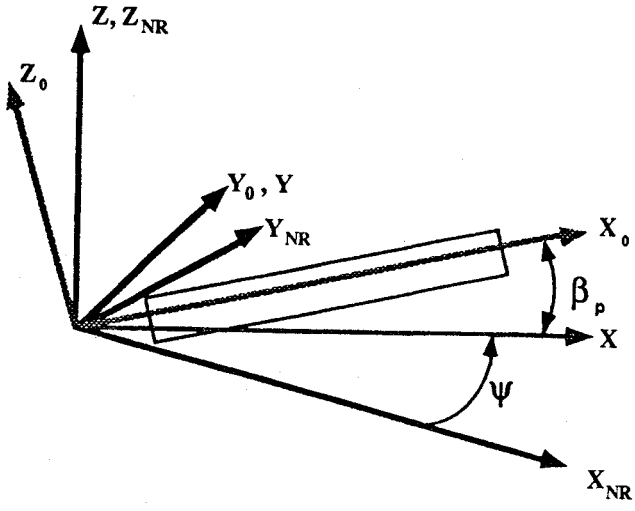

Fig. 2 Blade nonrotating, rotating, and preconed coordinate systems.

The sensitivity of the nonrotating inertia hub forces and moments to changes in the design parameter p is given by

$$\frac{\mathrm{d}\boldsymbol{F}_I}{\mathrm{d}p} = \underbrace{\frac{\partial \boldsymbol{F}_I(\psi)}{\partial p}}_{=\boldsymbol{d}_4} + \underbrace{\frac{\partial \boldsymbol{F}_I(\psi)}{\partial \overset{*}{\boldsymbol{q}}}}_{=\boldsymbol{D}_3}\underbrace{\frac{\partial \overset{*}{\boldsymbol{q}}}{\partial p}}_{=\boldsymbol{d}_2} + \underbrace{\frac{\partial \boldsymbol{F}_I(\psi)}{\partial \boldsymbol{q}}}_{=\boldsymbol{D}_4}\underbrace{\frac{\partial \boldsymbol{q}}{\partial p}}_{=\boldsymbol{d}_3} \tag{26}$$

$$\frac{\mathrm{d}\boldsymbol{M}_I}{\mathrm{d}p} = \underbrace{\frac{\partial \boldsymbol{M}_I(\psi)}{\partial p}}_{=\boldsymbol{d}_5} + \underbrace{\frac{\partial \boldsymbol{M}_I(\psi)}{\partial \overset{*}{\boldsymbol{q}}}}_{=\boldsymbol{D}_5}\underbrace{\frac{\partial \overset{*}{\boldsymbol{q}}}{\partial p}}_{=\boldsymbol{d}_2} + \underbrace{\frac{\partial \boldsymbol{M}_I(\psi)}{\partial \boldsymbol{q}}}_{=\boldsymbol{D}_6}\underbrace{\frac{\partial \boldsymbol{q}}{\partial p}}_{=\boldsymbol{d}_3} \tag{27}$$

The vectors $\boldsymbol{d}_2$ and $\boldsymbol{d}_3$ in Eqs. (26) and (27) are identical to the vectors $\boldsymbol{d}_2$ and $\boldsymbol{d}_3$ in Eq. (13).

The sensitivity vectors $\boldsymbol{d}_4$ and $\boldsymbol{d}_5$ can be obtained from the root load sensitivities. For example, the third element $\partial F_{zI}(\psi)/\partial p$ of the vector $\boldsymbol{d}_4$ is given by

$$\frac{\partial F_{zI}(\psi)}{\partial p} = \sum_{m=1}^{B}\left[-\frac{\partial P_{I3}^m(\psi)}{\partial p}\right] = \sum_{m=1}^{B}\left[-\frac{\partial F_{zI}^m(\psi)}{\partial p}\right] \tag{28}$$

where $P_{I3}^m(\psi)$ is the third component of the vector $\boldsymbol{P}_I^m(\psi)$ in Eq. (12) and the partial derivative $\partial F_{zI}^m(\psi)/\partial p$ is the third element of the vector $\boldsymbol{d}_1$ in Eq. (14).

Finally, matrices $\boldsymbol{D}_3$, $\boldsymbol{D}_4$, $\boldsymbol{D}_5$, and $\boldsymbol{D}_6$ are built from the rotating blade matrices using the fixed frame coordinate transformation. For example, the matrix $\boldsymbol{D}_4$ is

$$\frac{\partial \boldsymbol{F}_I(\psi)}{\partial \boldsymbol{q}} = \sum_{m=1}^{B}\begin{bmatrix} -\cos\psi_m & \sin\psi_m & 0 \\ \sin\psi_m & \cos\psi_m & 0 \\ 0 & 0 & -1 \end{bmatrix}\frac{\partial \boldsymbol{F}_I^m(\psi)}{\partial \boldsymbol{q}} \tag{29}$$

The matrices $\boldsymbol{D}_3$, $\boldsymbol{D}_5$, and $\boldsymbol{D}_6$ are built in a similar fashion.

Sensitivity of the Modal Load Vector

The derivation of the sensitivity of the modal load vectors is conceptually very similar to that of the blade root and hub loads described in the previous sections. The computer implementations of the respective calculations share a large portion of the coding. This section will focus again on the treatment of the inertia loads. The modal load vector is obtained by carrying out a modal coordinate transformation on the individual blade element load vectors, and then assembling the transformed load vectors. For example, the modal inertia load vector $\boldsymbol{I}$ for the blade is given by

$$\boldsymbol{I}(\boldsymbol{q}, \overset{*}{\boldsymbol{q}}; \psi) = \sum_{i=1}^{n_e} \boldsymbol{\Phi}_i \boldsymbol{P}_{Ii}(\boldsymbol{q}, \overset{*}{\boldsymbol{q}}; \psi) \tag{30}$$

in which $\boldsymbol{\Phi}_i$ is the portion of the normal mode matrix corresponding to the ith finite element, and $\boldsymbol{P}_{Ii}$ is the vector of nodal inertia loads for the ith element. The summation extends to all the n_e finite elements used to model the blade.

The sensitivity of the modal inertia vector to changes in a design parameter p is given by

$$\frac{\mathrm{d}\boldsymbol{I}(\boldsymbol{q}, \overset{*}{\boldsymbol{q}}; \psi)}{\mathrm{d}p} = \sum_{i=1}^{n_e}\left\{\underbrace{\frac{\mathrm{d}\boldsymbol{\Phi}_i}{\mathrm{d}p}}_{=\boldsymbol{D}_7}\boldsymbol{P}_{Ii}(\psi) + \boldsymbol{\Phi}_i\left[\underbrace{\frac{\partial \boldsymbol{P}_{Ii}(\psi)}{\partial p}}_{=\boldsymbol{d}_6} + \underbrace{\frac{\partial \boldsymbol{P}_{Ii}(\psi)}{\partial \overset{*}{\boldsymbol{q}}}}_{=\boldsymbol{D}_8}\underbrace{\frac{\partial \overset{*}{\boldsymbol{q}}}{\partial p}}_{=\boldsymbol{d}_2} + \underbrace{\frac{\partial \boldsymbol{P}_{Ii}(\psi)}{\partial \boldsymbol{q}}}_{=\boldsymbol{D}_9}\underbrace{\frac{\partial \boldsymbol{q}}{\partial p}}_{=\boldsymbol{d}_3}\right]\right\} \tag{31}$$

(The notation indicating the dependency of the nodal load vector $\boldsymbol{P}_{Ii}$ on the generalized coordinate vectors $\boldsymbol{q}$ and $\overset{*}{\boldsymbol{q}}$, has been dropped for simplicity.)

The matrix $\boldsymbol{D}_7$ in Eq. (31) is the sensitivity of the matrix of eigenvectors, or normal modes, to the design parameter p. For many typical rotary-wing aeroelasticity problems, the calculation of the natural frequencies and mode shapes of the blade represents only a very small fraction of the overall computational effort. Therefore it is convenient to calculate $\boldsymbol{D}_7$ numerically, using finite difference approximations.

The vector $\boldsymbol{d}_6$ in Eq. (31) is the sensitivity of the nodal inertia vector for the fixed normal modes and steady-state equilibrium position of the blade. To show this, consider the nodal inertia load vector for the ith element, which is given by

$$\boldsymbol{P}_{Ii} = \int_0^{l_i}\begin{Bmatrix} p_{yI}\gamma \\ p_{zI}\eta \\ [q_{xI} + v_{,x}\, q_{yI} + w_{,x}\, q_{zI}]\phi \end{Bmatrix}\mathrm{d}x \tag{32}$$

The vectors γ, η, and ϕ are vectors of Hermitian interpolation polynomials. The sensitivity vector $\boldsymbol{d}_6$ is given by

$$\boldsymbol{d}_6 = \frac{\partial \boldsymbol{P}_{Ii}}{\partial p} = \int_0^{l_i}\begin{Bmatrix} \dfrac{\partial p_{yI}}{\partial p}\gamma \\ \dfrac{\partial p_{zI}}{\partial p}\eta \\ \left[\dfrac{\partial q_{xI}}{\partial p} + v_{,x}\dfrac{\partial q_{yI}}{\partial p} + w_{,x}\dfrac{\partial q_{zI}}{\partial p}\right]\phi \end{Bmatrix}\mathrm{d}x \tag{33}$$

The structure of Eq. (33) is very similar to Eq. (14) and the derivatives are calculated in a similar way.

The vectors $\boldsymbol{d}_2$ and $\boldsymbol{d}_3$ in Eq. (31) are identical to the vectors $\boldsymbol{d}_2$ and $\boldsymbol{d}_3$ in Eq. (13). The matrices $\boldsymbol{D}_8$ and $\boldsymbol{D}_9$ in Eq. (13) are obtained in a fashion quite similar to that of $\boldsymbol{D}_2$ and $\boldsymbol{D}_3$ in Eq. (13) by reusing quantities that are already available as part of the analysis. Eqs. (10) and (11) show that the matrices $[\partial \boldsymbol{I}/\partial \boldsymbol{q}]^k$ and $[\partial \boldsymbol{I}/\partial \overset{*}{\boldsymbol{q}}]^k$ are calculated as part of the solution of the aeroelastic stability and response problem. For example,

$$\left[\frac{\partial \boldsymbol{I}}{\partial \boldsymbol{q}}\right]^k = \sum_{i=1}^{n_e}\boldsymbol{\Phi}_i\frac{\partial \boldsymbol{P}_{Ii}(\psi)}{\partial \boldsymbol{q}} = \sum_{i=1}^{n_e}\boldsymbol{\Phi}_i\boldsymbol{D}_8 \tag{34}$$

Therefore all the ingredients required to obtain the terms with $\boldsymbol{D}_8$ and $\boldsymbol{D}_9$ in Eq. (31) are available from the analysis, and only modest bookkeeping-type modifications to the computer program, and no additional computations, are required for the calculation of this portion of the sensitivities.

The sensitivities of the modal load vectors represent an important building block for the calculation of the sensitivities of the aeromechanic stability eigenvalues both in hover and in forward flight.

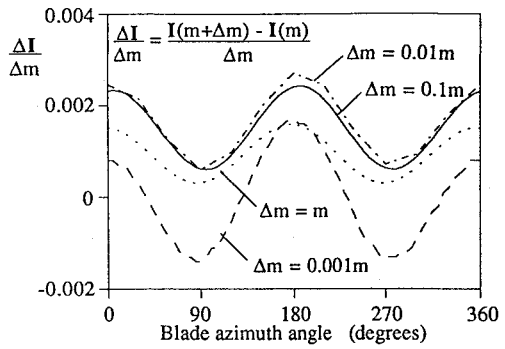

Fig. 3 Effect of finite difference step on the numerical calculation of $\partial I/\partial m = \lim_{\Delta m \to 0} \Delta I/\Delta m$ for the first flap mode.

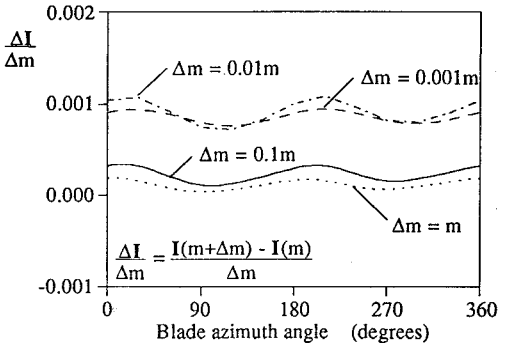

Fig. 4 Effect of finite difference step on the numerical calculation of $\partial I/\partial m = \lim_{\Delta m \to 0} \Delta I/\Delta m$ for the first lag mode.

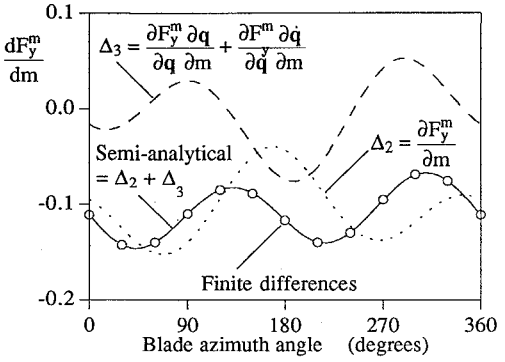

Fig. 5 Sensitivity of the inplane load F_{yI}^m to the distributed mass m and comparison with finite difference value; $\mu = 0.2$.

Results

The results presented in this section refer to a four-bladed hingeless soft-in-plane rotor configuration with fundamental rotating coupled natural frequencies of 0.71/rev and 1.14/rev in lag and flap, respectively. The blades have uniform mass and stiffness properties along the span. The thrust coefficient of the helicopter is $C_T = 0.005$ and the rotor solidity is $\sigma = 0.07$. The blade has no precone, built-in twist, or cross-sectional offset from the elastic axis. The rotor blade chord is $c = 0.055R$, the lift curve slope of the airfoil is $a = 6.28$, the profile drag coefficient of the airfoil is $c_{d0} = 0.01$, and the Lock number for the baseline case is $\gamma = 5.0$. The typical computer time required for one coupled trim solution and for an aeromechanic stability and response analysis are about 3 and 15 min, respectively, on a Sun SPARCstation 2.

Throughout this section, the sensitivities calculated using the semianalytical method are compared with those obtained using traditional finite difference techniques. For example, the sensitivity $\mathrm{d}I(p)/\mathrm{d}p$ of the inertia modal vector $I(p)$ can be calculated using finite difference approximations. If forward differences are used, one has

$$\frac{\mathrm{d}I(p)}{\mathrm{d}p} = \frac{I(p + \Delta p) - I(p)}{\Delta p} \tag{35}$$

where Δp is a small increment of the design variable p. The truncation error in Eq. (35) is $O[(\Delta p)^2]$. It is important that the increment Δp be small enough that the truncation error be negligible, but not so small that numerical cancellation problems may occur. Therefore, numerical experiments were conducted to determine a suitable value for the increment. Figures 3 and 4 are representative of the results of this preliminary investigation. They show the values of two components of the vector $\mathrm{d}I(p)/\mathrm{d}p$ as a function of the blade azimuth angle, for various values of the finite difference step Δp. The design parameter chosen is the value of the mass per unit span m, assumed to be constant along the blade. The inertia load vectors corresponding to both the baseline and the perturbed configuration are each obtained by performing a complete aeroelastic analysis, including calculation of the natural frequencies and normal modes, and of the coupled rotor-fuselage trim state. Figure 3 shows the second element of the sensitivity of the modal load vector which corresponds to the first flap mode and indicates that finite difference steps of 10% or 1% of the nominal value are small enough to generate accurate values of the derivatives. It should be noted that the curve representing a 0.1% step in the design parameter shows a significant deviation from the 1% and 10% curves, possibly indicating a numerical cancellation problem. However, Fig. 4, which shows the component of the sensitivity vector corresponding to the first lag mode, indicates that a smaller step size of 0.1% or 1% is needed to provide accurate estimates of the derivatives. Based on these results, and other results presented in Ref. 13, a value $\Delta p = 1\%$ was selected for all the finite difference-based calculations of the sensitivities.

Figure 5 shows the comparison of the finite difference approximation and the semianalytical method outlined in this paper for the rotating blade loads. The cost of calculating the sensitivity with respect to one design parameter, beyond that of the baseline analysis, is of one analysis for the finite difference method, and about 5% of one analysis for the semianalytical method. The finite difference approximation of each sensitivity is determined using a forward difference method as in Eq. (35) and is denoted by the open circles in the figure. The results obtained using the semianalytical method developed in this paper are represented by the solid curve in the figure and formed by summing the different components of the sensitivities from Eqs. (13), (26), (27), and (31) for the sensitivities of the blade root loads, the hub shears and moments, and the modal loads, respectively. For example, Fig. 5 shows the sensitivity of the rotating blade inertia load in the inplane direction to changes in mass. Now, Eq. (13) can be written as

$$\frac{\mathrm{d}F_y^m(\psi)}{\mathrm{d}m} = \underbrace{\frac{\partial F_y^m(\psi)}{\partial m}}_{=\Delta_2} + \underbrace{\frac{\partial F_y^m(\psi)}{\partial \dot{q}^*}\frac{\partial \dot{q}^*}{\partial m} + \frac{\partial F_y^m(\psi)}{\partial q}\frac{\partial q}{\partial m}}_{=\Delta_3} \tag{36}$$

The semianalytical method produces essentially the same results as the finite difference approximation, as indicated in the figure, but with a cost that is only slightly higher than one aeroelastic analysis for each design variable, and that increases much more slowly with the number of design variables. The components indicated with Δ_2 and Δ_3 can be interpreted as the contributions caused by the changes in inertia loads and steady-state equilibrium position, respectively. The figure suggests that the component Δ_2, which can be calculated for essentially no additional cost for some typical design parameters [see Eq. (17)], and for a very small cost for others, represents only part of the contribution to the sensitivity vector. The other component Δ_3 representing the contribution of the steady-state equilibrium position to the sensitivity vector also provides an important part of the sensitivity. Both components of the semianalytical derivatives are necessary to achieve accurate results. That implies that the gradients depend as much on the derivative of the inertia loads as on the effect of the change in mass on the trim condition.

The comparison of the finite difference approximation and the semianalytical method for the sensitivity of the hub loads to changes in the distributed mass m is shown in Fig. 6. Figure 6 shows the sensitivity of the hub load in the y direction (directed toward the right side). It appears that the primary contribution to the derivative is from the change in trim condition, that is, an increase of longitudinal flapping, whereas the direct contribution caused by the change in

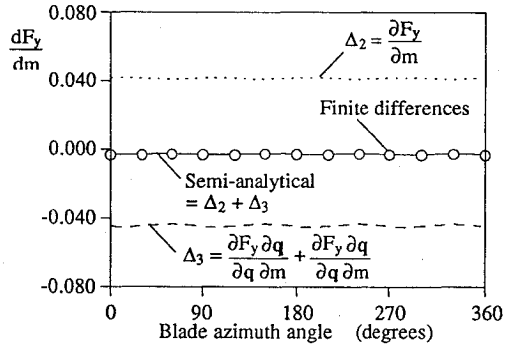

Fig. 6 Sensitivity of the lateral hub load F_{yI} to the distributed mass m and comparison with finite difference value; $\mu = 0.2$.

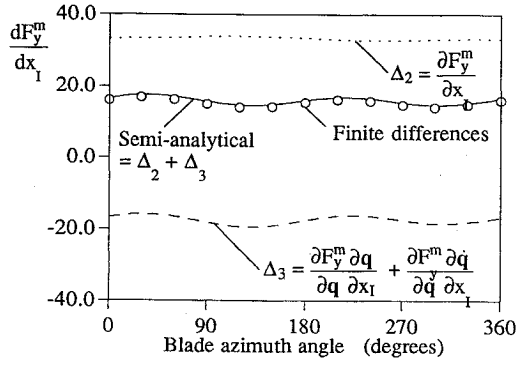

Fig. 7 Sensitivity of the inplane load F_{yI}^m to the chordwise offset of the center of mass from the elastic axis x_I and comparison with finite difference value; $\mu = 0.2$.

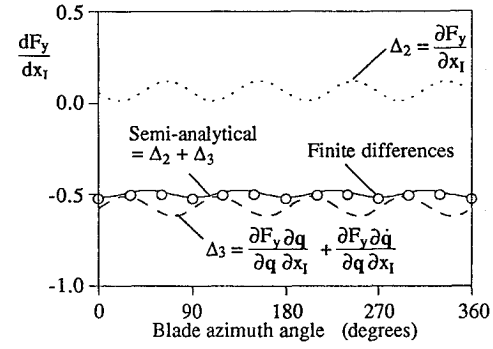

Fig. 8 Sensitivity of the lateral hub load F_{yI} to the chordwise offset of the center of mass from the elastic axis x_I and comparison with finite difference value; $\mu = 0.2$.

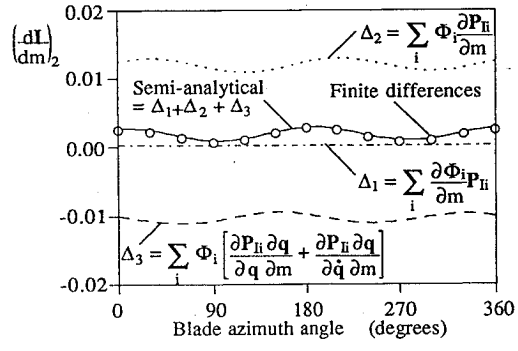

Fig. 9 Component of the sensitivity of the modal load vector, to the distributed mass m, corresponding to the first flap mode.

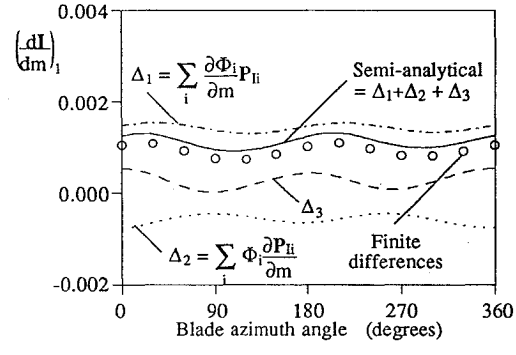

Fig. 10 Component of the sensitivity of the modal load vector, to the distributed mass m, corresponding to the first lag mode.

mass for fixed-blade steady response has a much smaller effect. In this case, both of the contributions to the semianalytic derivative play an important role. It is interesting to note that the two contributions are very close in magnitude and opposite in sign, resulting in a very small overall sensitivity of the sideward force F_y to changes in mass. The results presented here, together with other results that can be found in Ref. 13, indicate that the direct effects of mass changes on the hub loads generally have a sign opposite to that of the indirect effects that manifest themselves through changes in the equilibrium position of the blade. The former tend to increase the average hub loads, while the latter tend to decrease them. Both need to be included in the calculations of the semianalytical derivatives. Although a 4/rev variation is clearly visible in all the plots, the oscillatory component of the sensitivities is very small, indicating that changes in blade mass per unit span will mostly affect the steady values of the hub loads, but will not change the vibratory loads significantly. (This conclusion, however, is limited to uniform blades only.) The agreement between the finite difference-based and the semianalytical derivatives is excellent for all components of the hub loads.

Figure 7 shows the sensitivity of the rotating in-plane blade inertia loads to changes in the chordwise offset of the center of mass from the elastic axis x_I. Again, both components of the semianalytical derivative are necessary for accurate prediction of the sensitivity. The lateral hub load sensitivity is presented in Fig. 8 and shows that the steady portion of the lateral hub load is more sensitive to the changes in the trim condition caused by the change in x_I than it is to the changes in the inertial load. However, both components influence the 4/rev behavior of the sensitivity.

A comparison between the values of the sensitivity $\mathrm{d}\boldsymbol{I}(p)/\mathrm{d}p$ of the inertia modal vector $\boldsymbol{I}(p)$ calculated using a finite difference approximation and the semianalytical method is shown in Figs. 9 and 10. Figure 9 shows the element of the modal vector corresponding to the first flap mode and indicates that the semianalytic method produces essentially the same results as the finite difference approximation. The figure also shows the individual components that make up the sensitivity vector. In this case, the components indicated with Δ_2 and Δ_3 are supplemented by Δ_1, which can be interpreted as the contribution caused by the changes in the normal modes. The figure suggests that the components Δ_2 and Δ_3 represent the largest contributions to the sensitivity vector. The normal mode changes represent a negligible addition to the sensitivity vector. The element of the modal vector corresponding to the first lag mode is presented in Fig. 10. The semianalytical method again estimates the sensitivity derivative very well. The contribution caused by changes in the normal modes is still small, but is now of a size comparable to the other contributions, and therefore should not be neglected.

Figures 11 and 12 show the sensitivities of the modal structural loads to changes in the blade flap bending stiffness EI_2. Although the direct effect of the change in flap stiffness on the modal flap loads is seen in the shape of the curve in Fig. 11, the components containing the effects of the mode shape change and trim change permit the accurate prediction of the total derivative. A different conclusion is drawn regarding the effect of the flap stiffness change on the modal lag loads as shown in Fig. 12. In this case, the change in mode shape has very little effect on the total derivative, indicating that the structural lag loads can be accurately predicted by including

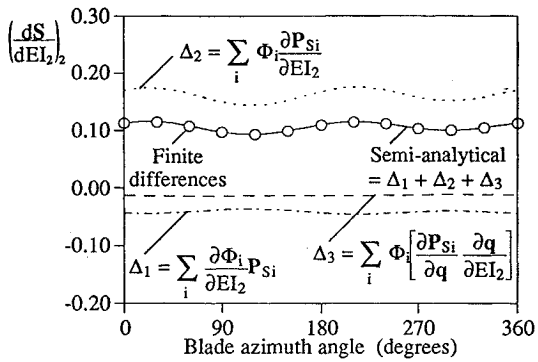

Fig. 11 Component of the sensitivity of the modal load vector, to the flap stiffness EI_2, corresponding to the first flap mode.

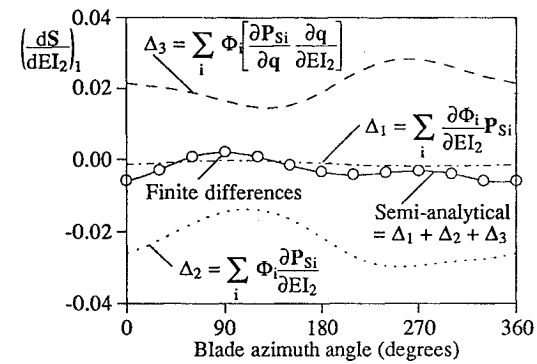

Fig. 12 Component of the sensitivity of the modal load vector, to the flap stiffness EI_2, corresponding to the first lag mode.

only the effects of the change in trim condition and the direct effects of the flap stiffness on the lag loads.

Conclusions

An efficient sensitivity analysis for rotary-wing aeromechanical problems has been developed. By exploiting the features of the implicit formulation of the elastic blade equations and the quasilinearization solution technique, the sensitivities of the modal, blade and hub inertia loads, and modal structural loads to changes in mass, center of mass offset, and flap bending stiffness can be efficiently determined. Examining the various components of the expression for the sensitivities, obtained through chain rule differentiation, reveals that the terms that are most expensive to obtain are already calculated as part of the basic analysis. Furthermore, it is relatively easy to update or modify the underlying mathematical model of the aircraft, because most of the changes that would then be required in the semianalytical sensitivities are already available once the basic analysis has been updated. The results of this study indicate that:

1) The semianalytical method dramatically reduces the required computational effort while producing results that are in excellent agreement with those generated using finite difference approximations.

2) Changes in mass and chordwise position of the center of mass affect rotor loads both directly, that is, through changes in the distributed forces and moments for fixed steady-state equilibrium position, and indirectly, through changes in the periodic response of the blades and in the trim conditions of the helicopter. Therefore, both types of effects need to be taken into account. This conclusion applies to both blade root loads in the rotating system, and hub loads in the fixed system. Changes in normal modes can be neglected, however, at least for uniform blades.

Acknowledgments

This work was supported by the Army Research Office, Contract No. DAAL-03-88-C-002, under technical monitor Tom Doligalski. Partial support was provided by the NSF Engineering Research Centers Program NSFD-CDR-88-03012.

References

[1]Friedmann, P. P., "Helicopter Vibration Reduction Using Structural Optimization with Aeroelastic/Multidisciplinary Constraints—A Survey," *Journal of Aircraft*, Vol. 28, No. 1, 1991, pp. 8–21.

[2]Various Authors, Special Issue of the *Journal of Aircraft*, "Multidisciplinary Optimization of Aeronautical Systems, Part II," *Journal of Aircraft*, Vol. 28, No. 1, 1991.

[3]Lim, J. W., and Chopra, I., "Response and Hub Loads Sensitivity Analysis of a Helicopter Rotor," *AIAA Journal*, Vol. 28, No. 1, 1990, pp. 75–82.

[4]Lim, J. W., and Chopra, I., "Stability Sensitivity Analysis of a Helicopter Rotor," *AIAA Journal*, Vol. 28, No. 6, 1990, pp. 1089–1097.

[5]Lim, J. W., and Chopra, I., "Aeroelastic Optimization of a Helicopter Rotor Using an Efficient Sensitivity Analysis," *Journal of Aircraft*, Vol. 28, No. 1, 1991, pp. 29–37.

[6]Lu, Y., and Murthy, V. R., "Sensitivity Analysis of Discrete Periodic Systems with Applications to Rotor Dynamics," *Proceedings of the AIAA/ASME/ASCE/AHS 32nd Structures, Structural Dynamics, and Materials Conference*, AIAA, Washington, DC, 1991, pp. 384–393 (AIAA Paper 91-1090-CP).

[7]He, C., and Peters, D. A., "Analytical Formulation of Optimum Rotor Interdisciplinary Design with a Three-Dimensional Wake," *Proceedings of the Fourth AIAA/USAF/NASA/OAI Symposium on Multidisciplinary Analysis and Optimization*, Vol. 2, AIAA, Washington, DC, 1992, pp. 1164–1176 (AIAA Paper 92-4778-CP).

[8]Celi, R., and Friedmann, P., "Rotor Blade Aeroelasticity in Forward Flight with an Implicit Aerodynamic Formulation," *AIAA Journal*, Vol. 26, No. 12, 1988, pp. 1425–1433.

[9]Celi, R., "Helicopter Rotor Blade Aeroelasticity in Forward Flight with an Implicit Structural Formulation," *AIAA Journal*, Vol. 30, No. 9, 1992, pp. 2274–2282.

[10]Spence, A., and Celi, R., "Coupled Rotor-Fuselage Dynamics in Turning Flight," *Proceedings of the AIAA Dynamics Specialist Conference*, AIAA, Washington, DC, 1992, pp. 292–301.

[11]Celi, R., "Hingeless Rotor Dynamics in Coordinated Turns," *Journal of the American Helicopter Society*, Vol. 36, No. 4, 1991, pp. 39–47.

[12]Spence, A. M., "A Design-Oriented Aeromechanical Analysis for Hingeless Rotor Helicopters in Straight and Turning Flight," Ph.D. Dissertation, Dept. of Aerospace Engineering, Univ. of Maryland, College Park, MD, May 1994.

[13]Celi, R., "Effect of Hingeless Rotor Aeroelasticity on Helicopter Longitudinal Flight Dynamics," *Journal of the American Helicopter Society*, Vol. 36, No. 1, 1991, pp. 35–44.